# Correlations between local flow mechanism and macroscopic rheology in concentrated suspensions under oscillatory shear

**ARTICLE** *in* SOFT MATTER · MARCH 2011

Impact Factor: 4.03 · DOI: 10.1039/C0SM00970A



**4 AUTHORS**, INCLUDING:

Wei Yu
Shanghai Jiao Tong University
**125** PUBLICATIONS **1,912** CITATIONS
SEE PROFILE

Yuanze xu
Xiamen University
**46** PUBLICATIONS **495** CITATIONS
SEE PROFILE

Soft Matter

View Online
Dynamic Article Links

Cite this: *Soft Matter*, 2011, **7**, 2433

www.rsc.org/softmatter

**PAPER**

# Correlations between local flow mechanism and macroscopic rheology in concentrated suspensions under oscillatory shear

**Ying Guo,[a] Wei Yu,*[a] Yuanze Xu[b] and Chixing Zhou[a]**

***Received 13th September 2010, Accepted 21st December 2010***
**DOI: 10.1039/c0sm00970a**



An optical visualization apparatus has been designed to measure the particle velocity of concentrated particle suspensions in a stress controlled rheometer equipped with a quartz parallel-plate. Suspensions with high and low matrix viscosity were used to investigate the nonlinear rheology and the local flow mechanism, as well as the correlations between particle velocity profiles and transition behaviors. Herein, it is shown that the sedimentation has great effects on the flow behavior of suspensions and on the particle velocity profiles. Local flow behaviors *e.g.* shear banding, drift in the center position of oscillatory shear and dynamic wall slip, have been studied comprehensively. By Fourier-transform rheology (FTR) analysis, the shear banding phenomenon is proved to be strongly linked with the nonlinear rheology of suspensions.

## I. Introduction

Suspensions, defined as heterogeneous fluids containing solid particles, usually exhibit complex flow behaviors and rheological properties. For example, on a large scale, great numbers of gravity-driven geophysical flows involve particle suspensions including sediment transport in oceans and rivers, debris flows, snow avalanches, mining slurries, mudflows and lahars. Small scale examples can be found in applications including batteries, solar cells, inkjet printing *etc.* The flow characteristics of these suspensions are believed to be reflected in the rheological properties. However, in the simplest situation where only hydrodynamic and contact interactions exist, the suspensions will exhibit complex rheological behaviors such as yield stress,[1–4] shear thinning, shear thickening/jamming[1] and thixotropy. Explaining these rheological behaviors are not so simple since there always appear other flow instabilities *e.g.* wall slip,[5–8] shear banding,[2,9,10] shear induced migration[4,5,11–13] and sedimentation[2,14–16] even in simple shear flow. For example, the coexistence of different local shear rates in the gradient direction of shear flow during the viscous flows of suspensions, which is the characteristic of gradient shear banding, indeed contradicts the common assumption of homogeneous flow, on which the typical rheological functions are defined. It means that apparent rheological functions include important information not only from the structures of materials but also from the status of flow inside the geometry. Shear banding is usually related to the structural evolution in materials, but also geometry-dependent. Shear banding in cone-plate geometry where the stress field is almost uniform could represent the structure of materials, while shear banding in Couette geometry, where the stress field is non-uniform, may be attributed to the stress gradient as well as the properties of materials. This suggests that the apparent rheological measurement using different geometries should be explained differently. Actually, these kinds of observations have inspired a lot of efforts[2,4,9,17–21] in recent years trying to understand the relationship between the rheology and the flow mechanism.

Unlike the rheometric measurement, studying the flow behavior is not so simple especially when it is coupled with a rheometer. Tracking the change of local elements is usually adopted to determine the flow behavior. Magnetic resonance imaging (MRI),[4,9,22] particle tracking velocimetry (PTV),[18,23–26] dynamic light scattering (DLS) and ultrasonic velocimetry (USV) are the most frequently used techniques in quantifying the velocity field.[27] As compared with other methods, the MRI technique has an advantage for the measurement of the velocity profile and local concentration simultaneously, which is very useful when there is a flow/gravity induced migration of particles. However, it is difficult to achieve both high spatial resolution and temporal resolution, and more importantly, no simultaneous rheological measurement can be performed at present. As an alternative, PTV has been proved very valuable in tracking the fluid pattern during and after flow. Although the local concentration could not be measured, PTV is able to visualize particle motion and state of aggregation directly with both high spatial resolution and temporal resolution. In addition, the PTV setup could be flexibly coupled with a commercial rheometer for simultaneous velocity and rheological measurements.

[a]*Advanced Rheology Institute, School of Chemistry and Chemical Engineering, Shanghai Jiao Tong University, Shanghai, 200240, P. R. China. E-mail: wyu@sjtu.edu.cn*
[b]*The Key Laboratory of Molecular Engineering of Polymers, Ministry of Education, Department of Macromolecular Science, Fudan University, Shanghai, 200433, P. R. China*

Among all the experimental modes that have been studied both for rheology and local flow behavior, steady shear is the most widely studied to produce the true shear stress-shear rate curve. Although the shear banding and local flow behavior can be obtained from a well-designed shear rate sweep by considering the yield stress of fluid and the stress gradient inside the Couette geometry,[17] it is still difficult to infer any information about the local flow in other geometries of parallel-plate or cone-plate, where the stress gradient in the shear gradient direction is missing. On the other hand, the local flow behavior under oscillatory shear is rarely investigated. In reality, the oscillatory shear, especially in a nonlinear regime, can reveal more information including the distortions from the sinusoidal waveform. The analysis of the latter by the frequently used Fourier transform rheology (FTR) or general stress decomposition (GSD)[28] technique will produce fruitful results which are still little understood. The occurrence of odd frequency components in the nonlinear region is sometimes related to structural changes or modifications,[3,29] and also as an indication of fluid inertia.[30] The appearance of even harmonics in the response signal may be attributed to wall slip.[31] The experimental insufficiencies[29,32] and the yield stress[3,33] are the other possible reasons for the occurrence of even frequency components. However, all the possible reasons mentioned above are established on the assumption of homogeneous flow of suspensions, which is not the case in many suspension flows. The analysis of higher harmonic contributions in oscillatory shear flow through PTV could characterize the local rheology of dense suspensions.

In this article we first study the macroscopic rheology of dense suspensions of non-Brownian particles using a controlled stress rheometer as described in Sec. III A. Then we use PTV to study the local flow mechanism and local rheology in Sec. III B, and also dynamic wall-slip responses in Sec. III C. Finally, the Fourier transformation is applied to the global and local signals in Sec. III D to find out the correlation between the nonlinear rheology and the flow behavior, and the conclusions are given in Sec. IV.

## II. Experimental section

### A. Materials and sample preparation

The suspensions consist of spherical particles dispersed in refractive index (RI) matched Newtonian fluid at different volume fractions. We use polymethylmethacrylate (PMMA) sphere (density $\rho_p = 1.2$ g cm$^{-3}$, RI = 1.4893, TOYOBO Co., Ltd.) as the disperse phase. The mean diameter ($d_p$) of particles is 80.43 μm with a polydispersity[34] of 0.003, measured with a Mastersizer 2000 laser particles size analyzer (Malvern Instruments Ltd., UK). To study the gravity effects on the local rheology, a Newtonian polydimethylsiloxane (PDMS, Tianyuan Group Shanghai Resin Factory Co., Ltd.) with high viscosity ($\eta_m = 120$ Pa s, $\rho_m = 0.97$ g cm$^{-3}$, RI = 1.4305 at 25 °C) and a Newtonian phenylmethylsilicone fluid (PMS, Brand *255#*, Shanghai Hualing Resin Co., Ltd.) with low viscosity ($\eta_m = 0.016$ Pa s, $\rho_m = 1.05$ g cm$^{-3}$, RI = 1.485 at 25 °C) were used as matrix, respectively. The matrices exhibits Newtonian behavior under all shear range of our study.

We studied the local and global rheological behaviors of the suspensions for a range of volume concentrations 40% < $\varphi$ < 57.5%, and most representative results shown here are obtained at 50% in PMS and 40%, 57.5% in PDMS. Before preparing the suspensions, the particles were dried in a vacuum oven for 24 h to remove residual water. All suspensions were prepared by mechanical mixing at speed of 100 rpm for 30 min until a homogeneous state was reached. The air incorporated during mixing was removed after resting for 24 h.

The maximum particle-based Reynolds number of suspensions is low ($R_{ep} = d_p v \rho_p/\eta_m \approx 10^{-6}$, where the maximum shear rate $\dot{\gamma}$ is about 12 s$^{-1}$ and the corresponding particle velocity $v$ is about 12 mm s$^{-1}$.) and the Péclet number is very high ($P_e = 6\pi\eta_m\dot{\gamma}r^3/k_BT \approx 10^9$, where the minimum shear rate is about $10^{-3}$s$^{-1}$, and $r$ is the particle radius, designated by 35.4 μm). Thus, the Brownian forces between the particles can be neglected. Consequently, the particle interactions considered here are of hydrodynamic interaction, and the inter-particle interactions include granular interactions and/or particle attractions, which are likely important as particles become close at high packing fractions. Due to the matrix-particle density difference, the settling velocity of a single PMMA particle in the suspensions was estimated to be about 469 μm h$^{-1}$ (50 vol%, PMS-system), 2.37 μm h$^{-1}$ (40 vol%, PDMS-system), 0.53 μm h$^{-1}$ (57.5 vol%, PDMS-system) according to Stokes' law ($U = d^2_p(\rho_p - \rho_m)g/18\eta_e$, where $\eta_e$ is the effective suspension viscosity).

Oscillatory stress amplitude sweep was performed to investigate the nonlinear properties and the transition behaviors. Suspensions were guaranteed to reach repeatable cycles at various stress amplitude. During the sweeps the primary sinusoidal stress signals were applied and the primary signals of shear strain were measured. The basic frequency of all amplitude sweeps was $f = 1$ Hz. The total sweep time was controlled within 3 h. However, it is well documented that the migration of particles depends greatly on the geometry of flow. Most evident migration phenomena were observed in Couette geometry and pressure-driven capillary/slit flow,[13,35] whereas the existence of migration in the parallel-plate geometry in oscillatory shear flow is still in dispute. Leighton and Acrivos[36] predicted radial migration of particles to the center of plates where the shear rate is zero, whereas recently Merhi *et al.*[37] did find evidence of shear-induced migration radially outward in both experiments and model prediction. On the other hand, little or no migration within the parallel-plate device was predicted by some models[38] and found in the traditional rheological measurements[39,40] or using powerful techniques like MRI.[12] Therefore, the shear-induced particle migration will not be the focus of this work. The sedimentation effects in the PMS-system should be considered, but it is considerably slight in the PDMS-system.

### B. Particle-tracking velocimetry setup (PTV)

Oscillatory sweeps were carried out on a stress-controlled Bohlin Gemini 200 rheometer at 25 °C. Quartz parallel-plate disks of 40 mm diameter were employed in the measurements. Although cone-plate geometry is preferred for its uniform shear rate, it is not used in the present study due to the relative large particle size. Dark PMMA particles (0.2 wt%, $d_p = 18.85$ μm, $\rho_p = 1.2$ g cm$^{-3}$, TOYOBO Co., Ltd.) embedded in the sample are tracked by passing a light sheet across the gap as shown in Fig. 1. The

 

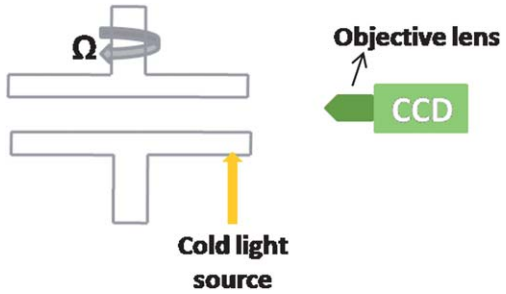


**Fig. 1** Schematic drawing of the particle-tracking velocimetry (PTV) apparatus.

movement of the tracer particles across the entire sample thickness is captured with a CCD camera (with a maximum speed of 93 frames per second with external trigger and full resolution). The CCD is mounted with a DIN objective lens (0.75X) through an adaptive tube. During analysis, the distance travelled by a particle can be determined by image analysis from different frames, from which the velocity profile at the edge of the quartz plate can be easily determined. The imposed shear stress was controlled at reasonable amplitudes to avoid the edge fracture and potential sample loss.

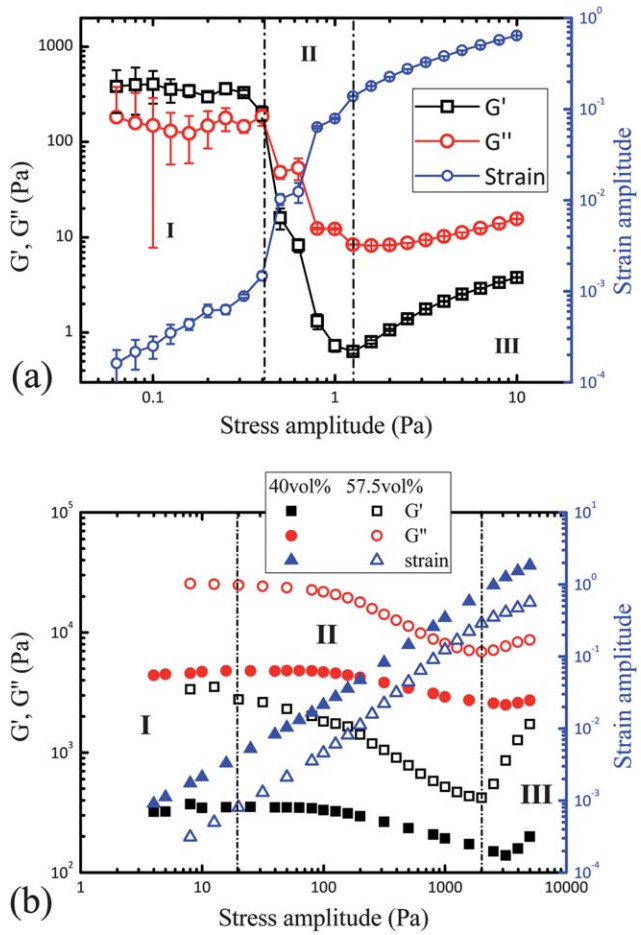


**Fig. 2** Stress amplitude sweep of the PMS-system (a), PDMS-system (b).

## III. Results and discussion

### A. Macroscopic rheology

The dynamic moduli from the stress amplitude sweep for the PMS-system and the PDMS-system are shown in Fig. 2. Apparently, both systems show similar stress dependence of dynamic moduli, from stress independency at low stress levels to shear thinning with a decrease in moduli at intermediate stress levels and finally to shear thickening with an increase in moduli at high stress levels. However, the differences between two systems are also evident. Firstly, $G'$ is larger than $G''$ in PMS-system at a low stress level, which suggests a solid-like behavior and a solid-to-liquid transition as the stress amplitude increases. However, viscous behavior dominates in PDMS-system with $G''$ always larger than $G'$. Theoretically, the stress of suspensions can be formally expressed as the sum of the contributions from the particle network and the matrix.[41–44] The viscoelastic contribution from interactions between particles[41–43,45] is usually considered as the main origin of the viscoelasticity of the suspension, which exhibits strong dependence on the particle concentration. The elastic moduli of suspensions increase monotonically with the particle concentration, from about 300 Pa (PDMS-system, 40 vol%) to about 400 Pa (PMS-system, 50vol%), and about 3000 Pa (PDMS-system, 57.5 vol%). The viscosity of Newtonian matrix has little effect on G′ of such suspensions, but influences the value of G″ greatly, which is as high as 4000 Pa for 40 vol% PDMS-system but only about 200 Pa for 50 vol% PMS-system. This is ascribed to the huge viscosity difference between PDMS and PMS. Thus, it is not difficult to understand that the particle network dominates the viscoelastic properties in PMS suspensions, while viscous behaviors are observed in PDMS suspensions.

Secondly, the transition stresses and the transition behaviors are completely different in two systems in regime II as shown in Fig. 2. $G'$ of PMS-system exhibits a sharp decrease over two decades and the strain amplitude increases over two decades within a rather small range of shear stress (0.4–1.6 Pa). This is the typical behavior known as the solid-to-liquid transition, where the initial stress of transition can be regarded as the dynamic yield stress (Fig. 2(a)). On the other hand, the modulus of the PDMS-system decreases mildly (less than one decade) and slowly in a wide range of shear stress (100–3000 Pa for 40% PDMS system and 20–2000 Pa for 57.5% PDMS-system) (Fig. 2(b)). The gradual transition in the PDMS-system suggests that the particle network is destroyed progressively. According to a simple analysis of the balance between the gravitational and the viscous stresses ($\eta\dot{\gamma} = \Delta\rho g d/2$),[2] the yield stresses of the two systems are almost in the same magnitude order of $10^{-1}$ Pa, which is close to the transition stress of the PMS-system but significantly lower than that of the PDMS-system. This is ascribed to the highly viscous matrix consuming a large portion of shear stress in the PDMS-system.

Finally, the two systems also show shear thickening behavior in regime III. Shear thickening is often ascribed to the origins of hydrodynamics[46] or dilation,[47–49] and expected to happen under certain conditions[1,50,51] including yield stress,[1] interparticle attractions[50] and volume fraction.[1,50] Here, the flow of our noncolloidal suspensions is dominated by the matrix viscosity,

and thus the inherent local flowing state of the shear thickening is totally different between the two systems due to the viscous dissipation. However, the shear thickening behaviors from the increasing modulus shown in Fig. 2 are hard to explain this way. We will show that the inherent local flow behaviors of both types of suspensions could be related to sedimentation as will be discussed later.

It is clear from Fig. 2 that the nonlinearity between stress amplitude and strain amplitude becomes more and more significant as the stress amplitude increases. Moreover, the appearance of nonlinear behavior is accompanied by the non-sinusoidal responses. As the higher harmonic signals emerge, the material functions such as $G'$ and $G''$ in the nonlinear region lose their original physical meaning. Considerable efforts[28,52–54] have been made towards obtaining useful and desirable material information from LAOS experiments. Graphical representations such as Lissajous-Bowditch curves (stress–strain or stress–strain rate) have been employed to describe the nonlinear response. Using the Lissajous-Bowditch curves, new measures were introduced by Ewoldt *et al.*[53] for accurately reporting the magnitudes of the viscoelastic modulus in the nonlinear regime, each of which has a distinct physical interpretation. For example, to capture the local elastic response of a material at small and large instantaneous strains $\gamma$, the first-harmonic elastic modulus $G'_1$ was decomposed as the minimum-strain/tangent modulus $G'_M$ at $\gamma = 0$ and the large-strain modulus $G'_L$ at the maximum imposed strain. Similarly, the first-harmonic loss modulus $G''_1$ was reconsidered through the introduction of the minimum-rate dynamic viscosity $\eta'_M$ and the large-rate dynamic viscosity $\eta'_L$. However, only odd harmonics are considered in these representations since the stress response is assumed to be of odd symmetry with respect to strain or strain rate. Even-harmonic terms can be observed in our two systems, and the appearance and growth of even harmonic contributions with stress amplitudes will be discussed in detail in Sec. D. The definitions of the above quantities lose their meanings because Lissajous–Bowditch curves become asymmetric when the even harmonics become evident.

The stress responses normalized by the imposed stress amplitude $\sigma_0$ are plotted in Fig. 3 with the normalized strain and strain rate, which was divided by the maximum strain $\gamma_m$ and strain rate $\dot{\gamma}_m$, respectively. Both the stress–strain curve and the stress–strain rate curve should be ellipses in a linear viscoelastic regime. It can be seen in Fig. 3(a) that Lissajous–Bowditch curves strongly deviate from elliptical behavior when the stress is as low as 0.2 Pa in regime I and are asymmetric when stress amplitude is smaller than 1.26 Pa. When the stress is larger than 1.58 Pa, which corresponds to the shear thickening regime shown in Fig. 2(a), stress attains symmetry with respect to strain or strain rate for the PMS-system. This is consistent with the sudden drop in even harmonics as shown in Fig. 12 below. The asymmetry at 0.2 Pa suggests that nonlinear behavior appears before the start of the transition of $G'$ at 0.4 Pa for the PMS-system. The distortion of the curves are usually more evident in viscous Lissajous–Bowditch curves (stress–strain rate curve) than that in elastic Lissajous–Bowditch curves (stress–strain curve). In regime III, secondary loops *via* self-intersection of Lissajous–Bowditch curves appear as the stress increases further.

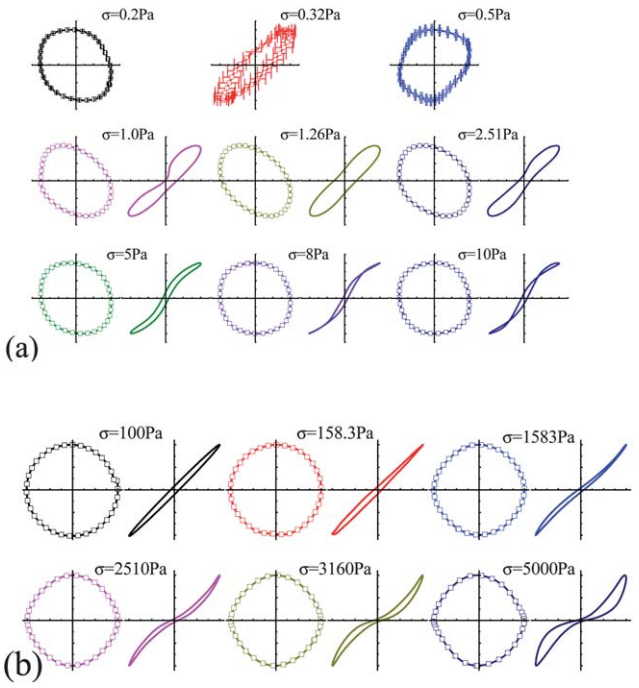


**Fig. 3** (a) The normalized Lissajous–Bowditch curves as $\sigma(t)/\sigma_0$ *vs.* $\gamma(t)/\gamma_m$ (solid lines with scatters) and $\sigma(t)/\sigma_0$ *vs.* $\dot{\gamma}(t)/\dot{\gamma}_m$ (solid lines) for PMS-system, 50 vol%. Stress–strain rate curves under low shear stresses are not shown due to the noisy data in strain rate. (b) The normalized Lissajous–Bowditch curves as $\sigma(t)/\sigma_0$ *vs.* $\gamma(t)/\gamma_m$ (solid lines with scatters) and $\sigma(t)/\sigma_0$ *vs.* $\dot{\gamma}(t)/\dot{\gamma}_m$ (solid lines) for PDMS-system with 57.5vol%.

However, Lissajous–Bowditch curves of the PDMS-system in Fig. 3(b) show different patterns. Viscosity dominant behavior can be found at the lower stress range from the nearly perfect elliptical stress–strain curve and thin ellipse in stress–strain rate curve in regime I. Evident deviation from elliptical behavior starts without self-intersection in the shear thickening regime when the stress increases in regime III. The viscous Lissajous–Bowditch curves of the PDMS-system in the thickening regime is completely different from that in the PMS-system. Although the self-intersection of viscous Lissajous–Bowditch curves was reported to be caused by a strong elastic-like nonlinearity,[55] it is unreasonable to explain the present results. Appearance of self-cross in stress–strain curve can be readily proved to be dependent on the phase angle of 1st harmonic and 3rd harmonic, and the relative intensity of 3rd harmonic ($I_{31}$). However, it is hard to draw any conclusion from that without information on the local flow behaviors.

### B. Local flow mechanism and local rheology

It has been mentioned above that suspensions exhibit very impressive differences in the macroscopic rheology relating to the sedimentation effects. However, it is obscure to interpret the macroscopic data without the knowledge of the local flow behavior. It is still unknown whether the differences in the global rheological behaviors come from the structural difference or the flow behavior. It is necessary to probe the local flow mechanism underlying the oscillatory shear. As one way to describe the local flow state of particles, PTV was used to analyze the velocity field

 

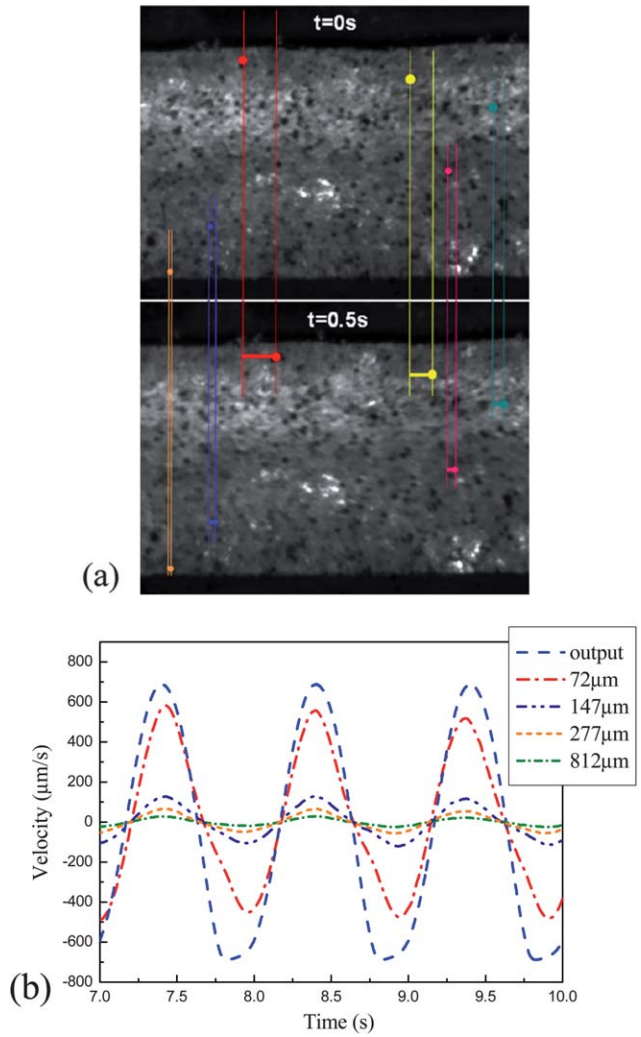


**Fig. 4** (a) Typical pictures from video recording of tracked moving particles in PMS-system at the initial state $t = 0$ s and transient state $t = 0.5$ s for an imposed stress amplitude of 1 Pa, where the distance between two plates is 1.1 mm. (b) The time dependent velocity of the tracked particles in (a). The position denotes the distance from the moving plate. The gap is 1.1 mm.

as a function of time and positions in the flow geometry. The measurements typically involve measuring the displacement of the tracked particles over different time of shear in the different layers across the sample thickness. A typical photo of the tracked particles and their time dependent velocity are shown in Fig. 4. The transient velocity measured by rheometer is also shown in Fig. 4(b) for comparison. It is clear that the maximum velocity decreases as the distance from the moving plate increases. Moreover, it is shown that there are little phase differences between the velocities at different positions. The phase differences are also absent between the particle tracking velocity and the output velocity, which is measured by the rheometer. The maximum velocities normalized by the peak velocity of the moving plate (normalized velocity) as a function of position normalized by the gap distance (normalized position) is shown in Fig. 5 and Fig. 6 to obtain the reduced local flow curves.

In Fig. 5, the normalized velocity profiles of the PMS-system shows the obvious shear banding as the stress amplitude increases, although the velocity below the critical shear stress 0.4 Pa is too low to be determined accurately. Two distinct regimes exist under lower shear stresses (<1 Pa), *i.e.*, the velocity decreases greatly in a regime close to the moving plate (small normalized position) while it keeps low values, and is almost constant at positions close to the stationary plate (large normalized position). As the shear stress becomes larger than 1 Pa, the velocity at large normalized positions gradually increases, and the discontinuity in the normalized velocity gradient gradually disappears. It is expected that a linear distribution of velocity across the gap will appear when the shear stress is high enough, although the velocity still shows a curved shape under the largest stress of 3.2 Pa in PTV experiments. The normalized velocity ($\tilde{V}$) presented in Fig. 5 can be well fitted by the following equation as a function of normalized position ($\tilde{h}$) to keep the continuity of velocity and velocity gradient

$$\tilde{V} = \begin{cases} \tilde{V}_c + a\left(\tilde{h}^2 - \tilde{h}_c^2\right) + \left(\tilde{V}'_c - 2a\tilde{h}_c\right)\left(\tilde{h} - \tilde{h}_c\right) & \tilde{h} < \tilde{h}_c \\ k_1\tilde{h} + k_2 & \tilde{h} > \tilde{h}_c \end{cases} \quad (1)$$

where $a$, $k_1$, $k_2$ are constant, $\tilde{h}_c$ is the normalized transition position, $\tilde{V}_c$ and $\tilde{V}'$ are the normalized velocity and velocity gradient at $\tilde{h}_c$, respectively. The shear rate across the gap can be obtained readily by differentiating eqn (1) with position, which also exhibits the local shear behaviors (right bottom plot in Fig. 5). The thickness of the sheared zone experiencing high shear rate shows a slight increase with stress amplitude during the solid–liquid transition. This discontinuity in the slope of the velocity profile seems to behave like the flow of a cement paste[56] in a Couette geometry, however, there is no stress gradient across the gap in the parallel plate geometry used in this work.

Contrary to the shear banding in PMS suspensions, suspensions with negligible settling velocity (PDMS system) exhibit the linear normalized velocity profile without shear banding but with evident wall slip at the moving and stationary plate, as shown in Fig. 6. The normalized velocity distribution of the highly concentrated suspension with 57.5 vol% is also shown with an apparent fitting line (dash-dot line) in Fig. 6. Apparently, the change of particle concentration has little effect on the velocity distribution in PDMS-system.

The development of shear banding and dynamic yield stress can find its origin in the competition between gravitational and viscous forces.[2] In other words, sedimentation could lead to the creation of a dense zone in which the particles are sufficiently densely packed that a yield stress emerges. Moreover, the shear-banding instability would occur when the hydrodynamic force is lower than the gravitational force, leading to the formation of contacts, which is reminiscent of the shear re-suspension mechanism.[57,58] According to the simple theory given by Fall *et al.*,[2] the critical shear rate $\dot{\gamma}_c$ for shear banding and the critical shear stress for the yield stress $\sigma_c$ could be estimated by $\eta\dot{\gamma} = \Delta\rho g d_p/2$ where $\Delta\rho$ is the density difference between particle and matrix. The critical shear rate from the PTV and experimental results are in good agreement with the simple theory for the PMS-system ($\dot{\gamma}_c = 0.017\ \mathrm{s}^{-1}$, $\sigma_c \approx 0.4$ Pa), and the sample undergoes no flow, shear banding and continuous shearing. However, the PDMS system experiences a different local flow mechanism since the critical shear rate ($\dot{\gamma}_c = 8.6 \times 10^{-5}\ \mathrm{s}^{-1}$) and shear stress ($\sim$1 Pa) is

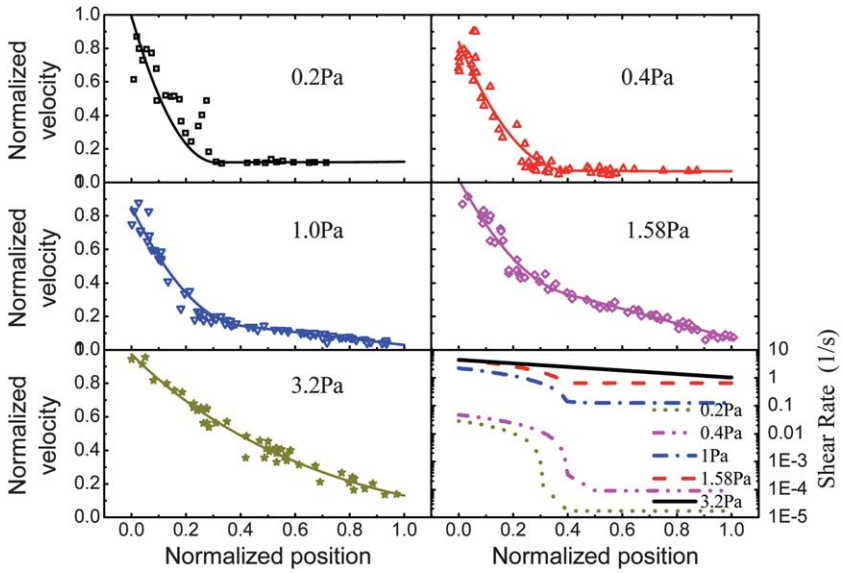


**Fig. 5** The experimental data of normalized velocity (colour symbols) fitted by eqn (1) (colour solid lines) for 50% PMS-system at stress 0.2 Pa, 0.4 Pa, 1 Pa, 1.58 Pa and 3.2 Pa. The bottom right graph is the plot of absolute shear rate derived from eqn (1) at dimensionless positions.

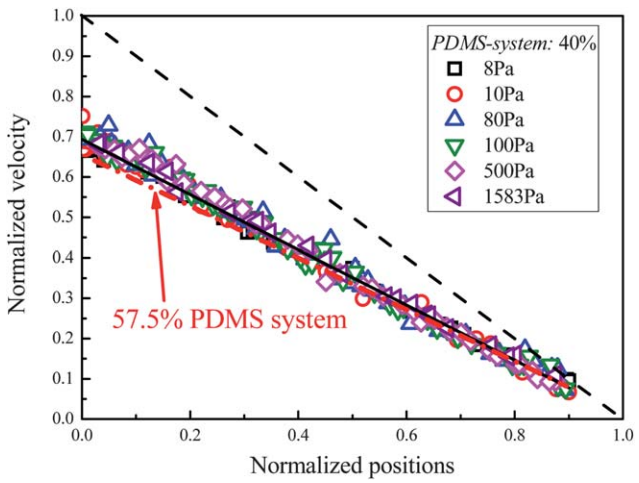


**Fig. 6** The normalized velocity profiles, evaluated from PTV in Fig. 2, of the PDMS-system across the normalized positions; solid line: apparent linear fit of the convergent velocity profile; dash line: the normalized velocity profile of Newtonian fluid; dash dot line: apparent linear fit of the reduced velocity profile for 57.5 vol%.

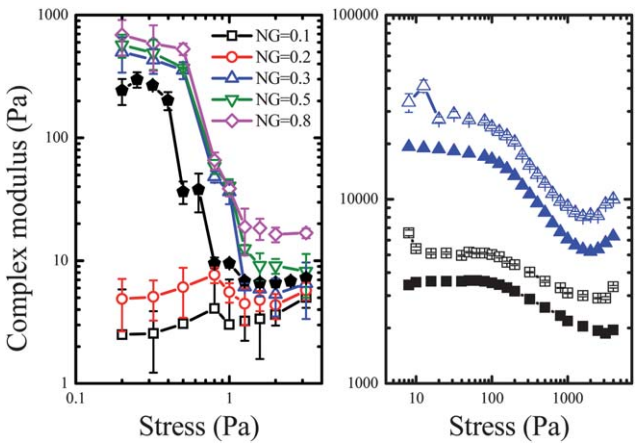


**Fig. 7** The position dependent complex modulus at different normalized positions (NP) for (right) 50% PMS-system and (left) PDMS-system: (triangle) 40%; (square) 57.5%. Filled symbol: macroscopic modulus measured with rheometry. Hollow symbol: local modulus calculated with PTV.

much lower than that of PMS-system. As the imposed shear rate or shear stress overcomes the critical amplitude, the viscous force dominates over gravity and the sample returns to being homogenous.

Combining the stress measurement by rheometer and the local flow measurement by PTV, it is possible to define the local or true rheological properties of materials. In oscillatory shear, the most important factors are the amplitude and the phase angle of the responses. The amplitude of local strain can be readily obtained from the local displacement, while the phase angle of the local strain is the same as the global one measured by rheometer since there is no phase difference between them (Fig. 4(a)). Since PDMS-system shows the linear continuous shearing profile, the local strain is position independent and the actual local strain in the sample is smaller than the global one that is measured by rheometer due to the wall slip effect. Under the assumption of homogeneous stress distribution, the local complex modulus ($|G^*(y)| = \sigma_0/\gamma_1(y)$) is deviated from the imposed stress $\sigma_0$ and the local strain amplitude $\gamma_1(y)$ to characterize the local rheological behavior (Fig. 7). It is then easy to understand that the local complex modulus should be position-independent and show the same stress dependency as the macroscopic modulus obtained by rheometer in the PDMS-system. However, the situation is quite different in the PMS-system. As mentioned above, the PMS-system shows several flow regimes varied with stresses. It is then expected that the strain amplitude also shows two different regimes, which are similar to that of the velocity profile and the shear rate distribution. The global strain amplitude from the rheometer is calculated from the ratio of the displacement of

 

the top plate to the gap distance, and lies in the intermediate position of the local strain profile, which suggests that the global strain amplitude is a kind of average of local strain. The local complex modulus can thus be determined, which exhibits a clear position dependency as shown in Fig. 7. Typically, the upper layer is close to the moving plate, suffers from more severe deformation and shows a very low modulus, whereas a clear shear-thinning transition with high suspension rigidity is found in the bottom shear layer that is close to the stationary plate. However, it should be stressed that although there is a big difference in the complex modulus at different positions under low stress level, all of them should demonstrate solid-like deformation no matter the absolute value of the complex modulus since the phase angle under low stress is smaller than $\pi/4$ which produce $G'$ higher than $G''$. The local rheology in the PDMS-system is believed to be the true one since the concentration is supposed to be homogeneous, while the local complex modulus obtained under different positions for the PMS-system cannot represent a true constitutive law due to the concentration profile induced by sedimentation. The macroscopic complex modulus is close to the local modulus at larger normalized positions, but falls between the local moduli of strong deformation regime and weak deformation regime.

From the macroscopic rheological behavior in Fig. 2(a), it is clear that as the stress amplitude becomes larger than 0.4 Pa there is a sharp increase in strain amplitude from $10^{-3}$ to $10^{-1}$ with an increase of phase angle, which apparently denotes a transition from solid-like behavior to liquid-like behavior. Therefore, it may be concluded that simultaneous change of strain amplitude and the phase angle can be used as the apparent criteria for the solid–liquid transition. However, it should be noted that change of the strain amplitude alone cannot be used to judge the solid–liquid transition. For example, the local strain amplitude could be as high as $10^{-1}$ in a strong shear regime even though the stress amplitude (0.2 Pa) is smaller than the critical transition stress shown in Fig. 2(a). This is ascribed to the strong plastic deformation of a solid-like material in the strong shear regime at a low stress amplitude of 0.2 Pa. Therefore, regime I in Fig. 2(a) does not have the typical meaning of a linear regime, where the stress amplitude and strain amplitude are directly proportional to each other and the waveform remains sinusoidal. Actually, strong nonlinear behaviors, such as the non-elliptic shape of the Lissajous curve and the strong plastic/weak elastic deformation in different shear banding zones, are shown in regime I. From the macroscopic point of view, regime II is a transition from solid-like behavior to liquid-like behavior due to the change of phase angle. Such transition happens only in the weak shear zone, and is not a global solid-to-liquid transition. Regime III in Fig. 2 represents apparent shear thickening which is usually explained as dynamic clustering or jamming across the gap. However, shear homogenization might be the other reason in this system since the velocity profile evolves to almost a straight line at high stress amplitude.

The other interesting phenomenon about the local flow is shown in Fig. 8. Usually, it is assumed that the particles will oscillate around an equilibrium position in the oscillatory shear flow. Such assumption is the basis of most analysis on the linear/nonlinear behavior under oscillatory shear. However, it is seen in Fig. 8 that under the applied stress amplitude of 1 Pa, the

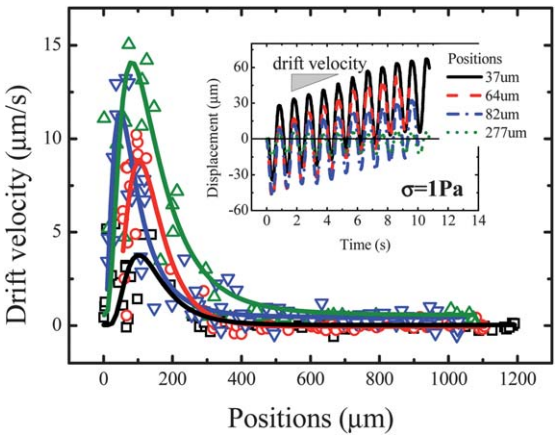


**Fig. 8** The drift velocity of PMS-system derived from different positions as a function of stress (square) 0.4 Pa, (circle) 0.63 Pa, (down-triangle) 0.8 Pa, (up-triangle) 1 Pa. Inset: The displacement *vs.* time at different positions for PMS-system at stress 1 Pa.

displacement of a tracing particle will oscillate around an equilibrium position when it is far from the moving plate in the weak shear regime, while it will oscillate with a drift of equilibrium position when it is close to the moving plate. The drift velocities can be defined from the slope of the time-dependent center position of the oscillation, which are clearly shown in the inset of Fig. 8. It is noticed that the drift of oscillatory position only appears in regime II of the PMS-system (Fig. 2(a)). There is no apparent drift of oscillatory position in regime I and regime III of the PMS-system, and no drift in the PDMS-system where shear banding is not observed. Moreover, the drift of oscillation position only appears in the layer close to the moving plate, *i.e.*, the strong deformation regime, but there is a peak drift velocity lying in the center of the strong deformation regime. It is also found that the maximum drift velocity increases first as the stress increases and enters regime II, then decreases and vanishes as the stress increases further and enters into regime III. The appearance of the drift of oscillation position is consistent with the transition from the solid-like to liquid-like behavior. Such behavior is ascribed to the thixotropic behavior of the PMS suspension in the transition regime. However, such local flow behavior is shown neither in the drift of global displacement, nor in the change of waveform of displacement (as shown in Sec. III D).

### C. Wall slip

It has been shown that the samples suffered from wall slip during shear (Fig. 4–Fig. 6). Wall slip in polymer melts and solutions has been a constant experimental theme and extensively studied using a variety of setups and methods.[31,59–65] Almost all of the investigations of wall slip for suspensions have followed the slip theories of polymer melts/polymeric suspensions, such as entangled DNA solution,[25] ethylene Glycol and cornstarch suspensions,[59] KCl/elastomer suspensions.[62] The central task of these attempts is to find the relationship between slip velocity $u_s$ and shear stress $\sigma$, and some useful relations, *i.e.*, exponential model[64] and "memory slip model"[31] were proposed. In most of those studies, however, the wall slip velocities were inferred from

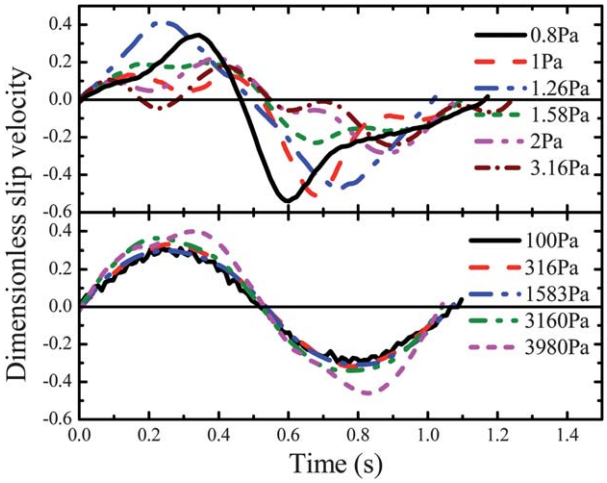


**Fig. 9** Dimensionless transient slip velocities at the moving plate as a function of time and applied stress amplitudes; (top): 50 vol%, PMS-system; (bottom): 40 vol%, PDMS-system.

the viscometric experiments, which were then analyzed on the basis of these model equations, rather than through direct velocity measurements within the suspensions. Jana and co-workers[63] first used a laser Doppler anemometer to determine the apparent wall slip velocity coefficient of concentrated suspensions through measuring the particle velocity across the Couette gap. Under steady shearing conditions, they found the slip coefficient was insensitive to the magnitude of the applied shear rate and dependent on the relative effective viscosity of the suspension with respect to that of the pure fluid. However, less effort was made towards obtaining the slip functions of the concentrated suspensions under oscillatory shear experiments. With the help of PTV, the transient wall slip velocity of the suspensions under oscillatory flow can be readily obtained from Fig. 4.

The transient slip velocity at the moving wall ($u'_s$) calculated from the edge velocity ($v_0$) and the particle tracking velocity ($v$) was normalized by maximum edge velocity ($V_0$), as shown in Fig. 9. The dimensionless transient slip velocity at the moving

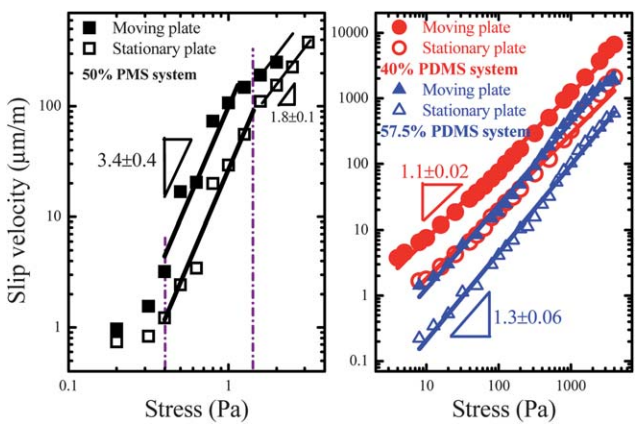


**Fig. 10** The maximum slip velocity on both moving (solid symbols) and stationary wall (hollow symbols) as a function of stress for 50 vol% PMS-system (squares), 40 vol% PDMS system (circles), 57.5 vol% PDMS system (triangles). Solid line: apparent linear fit of the slip velocity *vs.* stress using the relation $U_s \propto \sigma^n$.

plate ($u'_s$) exhibits the periodic asymmetric responses for the PMS-system, whereas suspensions with high matrix viscosity (PDMS-system) display quasi-symmetric slip responses. Besides the slip at the moving plate, weaker slip behavior was also exhibits on the stationary wall ($u''_s$). The maximum slip velocity both at the moving ($U'_s$) and stationary plate ($U''_s$) as a function of stress are plotted in Fig. 10. It should be pointed out here that the maximum slip velocity is the mean value due to the periodic asymmetric responses. As shown in Fig. 10, there is a common feature existing between the PMS-system and the PDMS-system, namely higher $U'_s$ than $U''_s$, which coincides with the results of glass beads suspensions[6] and Carbopol gel.[21] Aral and Kalyon[6] attributed the different slip velocities to the strong coupling between wall slip and viscoplasticity in the viscoplastic region and the emergence of sedimentation effect introduced by prolonged shearing in the viscous flow region. Although the settling effect of PDMS-system is considerably smaller than that of PMS-system, wall slip often occurs in a very thin binder-rich layer and a thicker slip layer of the PDMS-system near the moving surface introduced by a slight sedimentation would lead to a higher slip velocity on top plate than that on the bottom plate. On the other hand, considerable difference in the stress dependence of the slip velocity can be found between the PMS-system and the PDMS-system in Fig. 10. In the PDMS-system where there is no shear banding, the slip velocity ($U'_s$ and $U''_s$) increases with stress with the power law exponent ($n$) about $1.1 \pm 0.02$ for concentration 40 vol% and $1.3 \pm 0.06$ for 57.5 vol% ($U_s \propto \sigma^n$). Besides the stress dependence of slip velocity, it also depends on the concentration of the particles. The more concentrated suspension 57.5 vol% shows the lower slip velocity, as shown in Fig. 10. The mechanism of slip flow for concentrated suspensions involves the formation of binder-rich slip layer with a characteristic thickness of $\delta$. A thicker slip layer or smaller binder viscosity ($\eta_m$) gives rise to a greater wall slip velocity. Kalyon[62] suggested a correlation between the slip layer thickness over the particle diameter ratio, $\delta/d_p$, *versus* the ratio of the volume concentration of the particles over their maximum packing fraction, $\varphi/\varphi_m$ for the homogenous material. The mean apparent slip layer thickness was calculated as 30.2 μm for 40 vol% and 8.2 μm for 57.5 vol%, with $d_p = 80.45$ μm and $\varphi_m = 0.64$. Thus, it is reasonable to obtain a higher slip velocity in the less concentrated system.

However, the slip behavior is quite different in the PMS-system, where strong shear banding has been observed. Generally, the slip velocities on both surfaces show the same stress dependence with a higher slip velocity on the top plate. An interesting phenomenon is the evident discontinuity of the slip velocity on the both plates at 0.4 Pa and 1.6 Pa, corresponding to the transition from regime I to II and regime II to III in rheology (Fig. 2(a)). The stress dependent slip velocities show a larger power law exponent in regime II ($n = 3.4 \pm 0.4$) than regime III ($n = 1.8 \pm 0.1$). Below the yield stress, the suspension just slips at both walls with elastic-like deformation. The wall slip effects observed in regime I, indicate strong coupling between wall slip and viscoplastic behavior. After yielding, the suspension enters into a severe shear banding regime, namely a transition region, which indeed shows a sudden rise of slip velocities with stress while the slip layer thickness keeps constant on the both plates. Although the sample is heterogeneous across the gap, it remains locally homogenous in the individual shear bands with certain

 

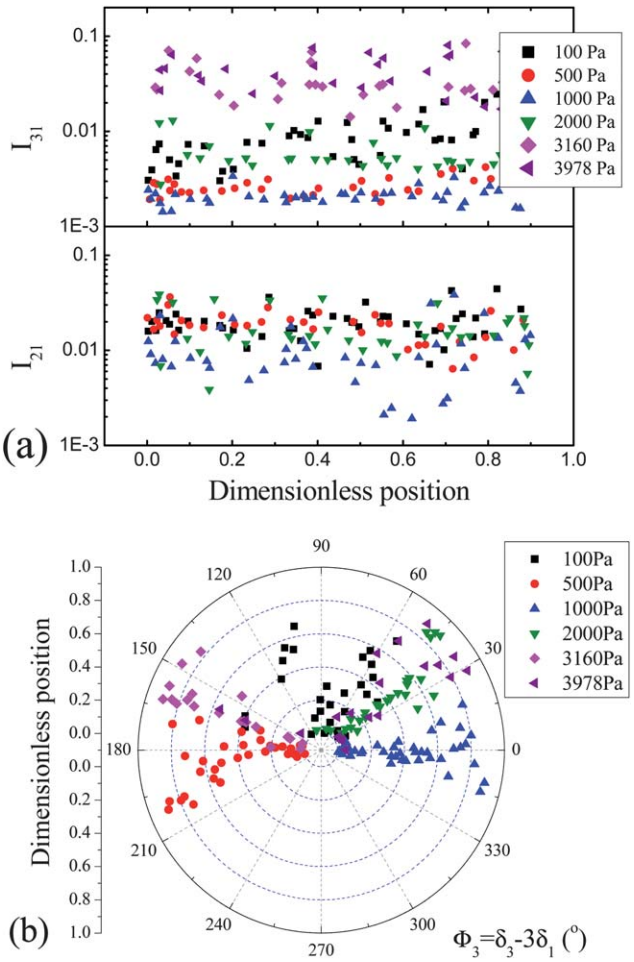


**Fig. 11** Representative results of (a) the relative second (bottom) and third (top) harmonic and (b) the relative phase angles across the dimensionless gap as a function of the stress amplitudes for 57.5 vol%, PDMS-system, according to particle tracking.

local concentrations. This is consistent with the evolution of the local complex modulus of PMS-system with stress in Fig. 7, where the rigidity of sample keeps unchanged within shear bands. According to the correlation of $\delta/d_p = 1 - \varphi/\varphi_m$, the slip layer thickness of both bands should remain unchanged. As the stress increases above 1.6 Pa, the viscous force is becoming dominant over the gravity force and the sample returns to being homogenous through a shear-induced re-suspension[58] mechanism, hence the slip layer thickness remains stable and the power law exponent becomes smaller than that in regime II. Moreover, it is noticed that the scaling exponent in the transition regime is much larger than the usual observation. Such strong dependence of slip velocity on stress cannot be explained only by the vertical concentration gradient, but is believed to be related to the structures of the suspensions.

### D. Fourier-transform rheology (FTR) and local flow

The macroscopic rheology and local flow behaviors have been shown in the previous sections. The connection between them, however, cannot be completely established just from the amplitude of the deformation, as shown by the local rheology in Fig. 7. Quantitative analysis of the shape of waveform could be a possible bridge to connect them. As the most common method of quantifying nonlinear oscillatory experiments, FTR has been extensively applied in different systems.[3,24,28,52,66] The mathematical procedures of Fourier transform results in a power spectrum of frequency where the fundamental and higher order harmonics appear. The most important higher order harmonics are the odd ones, which keeps the regular periodicity of the oscillation. These non-linearities are often believed to depend on the structures of materials. Each peak of odd harmonics in a power spectrum of strain is described by a magnitude $I_n$ and a phase angle $\varphi_n$. One way to quantify the degree of non-linearity is the ratio of intensities ($I_{n/1} = \gamma_n/\gamma_1$) of the nth-harmonic ($I_n$) to the 1st-harmonic ($I_1$). The emergence of the even-harmonic terms are always ascribed to some "experimental errors", such as instrumental errors, secondary flows,[67] or dynamic wall slip (memory slip).[31] Considering the complex local flow behaviors in suspensions, there might be additional causes for the occurring of even harmonics. With the aid of PTV, particle transient velocities across the gap were recorded. Meanwhile, the raw data of output strain signals were sampled as suspensions attained its steady state. The nonlinear behavior from macroscopic rheology and local flow will be compared with each other.

The first problem is whether the nonlinearity is position dependent. The variations of the $I_{21}$ and $I_{31}$ across the gap distance were examined through the particle tracking as presented in Fig. 11. As shown in Fig. 11, both the nonlinear intensities and the phase angles show the gap independence for PDMS suspensions. Similar results have been observed for PMS suspensions, where there is shear banding. The position independency of nonlinearity suggests that stress amplitude is the only important factor here.

The third harmonics are quite evident under all imposed stresses, while the second harmonics only appears under certain stresses. The relative intensities of the higher harmonics are shown in Fig. 12 for 50% PMS suspension and 57.5% PDMS suspension. It should be noted that the only difference between the macroscopic and the local waveform is the dynamic wall slip, *i.e.*, the local nonlinearity represents the structures of the

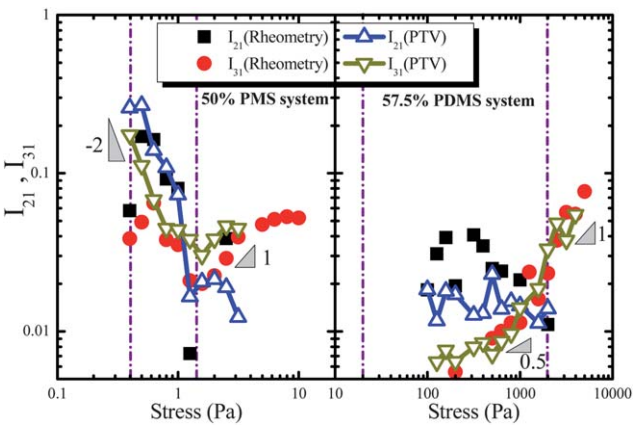


**Fig. 12** Relative intensities of the 2nd and 3rd harmonics under different stress amplitudes from the particle tracking (hollow scatters) and rheological measurement (solid scatters) for (right) 50 vol% PMS suspension; (left) 57.5 vol% PDMS suspension.

materials only, while the macroscopic one is the collective contributions from the structures of materials and the wall slip.

For PMS suspension, both $I_{21}$ and $I_{31}$ decrease with the increase of stress in regime II with the scaling law $I_{21} \propto I_{31} \propto \sigma_0^{-2}$, and the local nonlinearity is well consistent with the macroscopic one. This suggests that wall slip does not contribute to the nonlinear intensities in the transition regime (II). Moreover, the same intensity of the second harmonic between local displacement and macroscopic strain means that the even harmonic in the PMS suspension may be related to the inhomogeneous structures of the suspensions. As the shear stress increases further into the shear thickening regime (III), $I_{21}$ in the macroscopic strain disappear immediately, while $I_{21}$ in the local displacement still exists at a constant level and vanishes at larger stress. The difference of the even harmonic in regime III can only be ascribed to the existence of wall slip. In reality, the even harmonic contribution due to the yield stress becomes weaker as the shear stress increases and the Leighton number, $Le = \eta_s\dot{\gamma}/\sigma_y$, becomes much larger than 1. The immediate disappearance of $I_{21}$ in the macroscopic strain as the stress enters into regime III is then ascribed to the cancellation of intensities owing to the difference in phase angle of even harmonics between the local displacement and the displacement due to the dynamic wall slip. However, the contribution of dynamic wall slip is hard to obtain even with the high resolution PTV method in this study since the dynamic slip velocity as shown in Fig. 9 is still too noisy to resolve accurate phase angle. In the shear thickening regime, local $I_{31}$ from PTV measurement is a little bit higher than that measured by rheometer, and both of them increase with the stress *via* $I_{31} \propto \sigma_0$. It is noticed that such scaling is different from that observed for polymers where the scaling exponent is around 2 depending on the chain topology, but similar to that of polymer composites.[28]

The nonlinearity in PDMS suspension shows another pattern. $I_{21}$ of macroscopic strain and local displacement are almost constant in the regime II and disappear in regime III, but the macroscopic one is obviously larger. Since there is no shear banding in the PDMS suspension, the difference in $I_{21}$ is attributed to the dynamic wall slip. The third harmonics of the macroscopic strain and the local displacement agree with each other very well, and follow the scaling law $I_{31} \propto \sigma_0^{0.5}$ in regime II and $I_{31} \propto \sigma_0$ in regime III. It seems that wall slip would not affect the odd harmonics in PDMS suspensions.

On the other hand, the nonlinearity is generally smaller in the PDMS-system than that in the PMS-system, especially in regime II. This could be explained by the relative ratio between the viscosity $\eta$ in liquid-like state and the modulus $G$ in solid-like state. It is shown by Yu *et al.*[28] that the nonlinearity is determined by $\eta\omega/G$ for a Bingham fluid, where $\omega$ is the oscillating frequency. The higher $\eta\omega/G$, the smaller $I_{n1}$. For suspensions with the same kind of particles but a different matrix, the modulus in the solid-like state is determined by the inter-particle distance and friction between particles, and should depend on the concentration of particles. The viscosity, however, depends on the viscosity of matrix fluid as well as the hydrodynamic interactions of particles. It is expected that the ratio $\eta\omega/G$ is higher for PDMS-system due to the high viscosity of PDMS, which implies that the nonlinearity in PDMS-system will be weaker than that in PMS-system.

When comparing the nonlinearity of the PMS suspension and the PDMS suspension, it is clear that the main difference exists in regime II. Sharp decline of high harmonics in regime II is associated with the change from solid like to liquid like behavior, and related to the yield stress and shear banding behavior. However, constant or weak increase of high harmonics in regime II suggests viscous dominating flow in the suspensions, no evident yield transition and no shear banding. The contribution of dynamic wall slip to $I_{31}$ is quite limited in oscillatory shear, which suggests that the third harmonic could be a good parameter to study the structures of suspensions.

## IV. Conclusions

The development of shear banding is shown even in the homogeneous stress field, and the sedimentation effect caused by the competition between gravitational and viscous forces is responsible for the development of a dynamic yield stress and of shear banding in granular suspensions. The localization of shearing contributes to the transition behaviors of macroscopic rheology, whereas continuous shearing with the linear and nonlinear velocity profiles could result in the totally different global rheology. To probe the local flow mechanism, PTV and Fourier transformations were employed to analyze the macroscopic/local rheological responses and the local velocities, namely, global FTR and local FTR. By comparing the macroscopic nonlinear rheological behaviors with the nonlinear local flow it is found that the third harmonic can be used to represent the structural change in the suspension, which is less affected by the dynamic wall slip. The stress dependency of high harmonics can be a good indicator on the effect of yield stress, wall slip and the shear banding behavior. However, not all the local flow mechanisms can be reflected in the nonlinear intensities of macroscopic rheology.

## Acknowledgements

The authors acknowledge financial support for this work from the *National Natural Science Foundation of China* (No. 50930002) and Shanghai Leading Academic Discipline Project (No. B202). W. Yu is supported by the SMC project of Shanghai Jiao Tong University.

## References

1 E. Brown and H. M. Jaeger, *Phys. Rev. Lett.*, 2009, **103**, 086001.
2 A. Fall, F. Bertrand, G. Ovarlez and D. Bonn, *Phys. Rev. Lett.*, 2009, **103**, 178301.
3 Y. Guo, W. Yu, Y. Xu and C. Zhou, *Phys. Rev. E: Stat., Nonlinear, Soft Matter Phys.*, 2009, **80**, 061404.
4 G. Ovarlez, F. Bertrand and S. Rodts, *J. Rheol.*, 2006, **50**, 259–292.
5 M. Allende and D. M. Kalyon, *J. Rheol.*, 2000, **44**, 79–90.
6 B. K. Aral and D. M. Kalyon, *J. Rheol.*, 1994, **38**, 957–972.
7 U. Yilmazer and D. M. Kalyon, *J. Rheol.*, 1989, **33**, 1197–1212.
8 T. Q. Jiang, A. C. Young and A. B. Metzner, *Rheol. Acta*, 1986, **25**, 397–404.
9 N. Huang, G. Ovarlez, F. Bertrand, S. Rodts, P. Coussot and D. Bonn, *Phys. Rev. Lett.*, 2005, **94**, 028301–028304.
10 P. Schall and M. van Hecke, *Annu. Rev. Fluid Mech.*, 2010, **42**, 67–88.
11 D. J. Pine, J. P. Gollub, J. F. Brady and A. M. Leshansky, *Nature*, 2005, **438**, 997–1000.
12 A. W. Chow, S. W. Sinton, J. H. Iwamiya and T. S. Stephens, *Phys. Fluids*, 1994, **6**, 2561–2576.
13 J. R. Abbott, N. Tetlow, A. L. Graham, S. A. Altobelli, E. Fukushima, L. A. Mondy and T. S. Stephens, *J. Rheol.*, 1991, **35**, 773–795.

 

14 W. J. Tseng and C. H. Wu, *Ceram. Int.*, 2003, **29**, 821–828.
15 W. C. K. Poon, L. Starrs, S. P. Meeker, A. Moussaid, R. M. L. Evans, P. N. Pusey and M. M. Robins, *Faraday Discuss.*, 1999, **112**, 143–154.
16 A. J. C. Ladd, *Phys. Fluids*, 1997, **9**, 491–499.
17 G. Ovarlez, S. Rodts, A. Ragouilliaux, P. Coussot, J. Goyon and A. Colin, *Phys. Rev. E: Stat., Nonlinear, Soft Matter Phys.*, 2008, **78**, 036307.
18 P. E. Boukany and S.-Q. Wang, *Soft Matter*, 2009, **5**, 780–789.
19 P. Coussot, L. Tocquer, C. Lanos and G. Ovarlez, *J. Non-Newtonian Fluid Mech.*, 2009, **158**, 85–90.
20 G. Ovarlez, S. Rodts, X. Chateau and P. Coussot, *Rheol. Acta*, 2009, **48**, 831–844.
21 T. Divoux, D. Tamarii, C. Barentin, S. Manneville and Bastien, *Phys. Rev. Lett.*, 2010, **104**, 208301.
22 P. Coussot, *Rheometry of pastes, suspensions, and granular materials*, John Wiley & Sons, New York, 2005.
23 Y. T. Hu and A. Lips, *J. Rheol.*, 2005, **49**, 1001–1027.
24 S. Ravindranath and S.-Q. Wang, *J. Rheol.*, 2008, **52**, 341–358.
25 P. E. Boukany, Y. T. Hu and S.-Q. Wang, *Macromolecules*, 2008, **41**, 2644–2650.
26 Y. T. Hu, C. Palla and A. Lips, *Macromolecules*, 2008, **41**, 6618–6620.
27 S. Manneville, *Rheol. Acta*, 2008, **47**, 301–318.
28 W. Yu, P. Wang and C. Zhou, *J. Rheol.*, 2009, **53**, 215–238.
29 H. Komatsu, T. Mitsui and S. Onogi, *J. Rheol.*, 1973, **17**, 351–364.
30 J. Dunwoody, *J. Non-Newtonian Fluid Mech.*, 1994, **53**, 83–98.
31 M. D. Graham, *J. Rheol.*, 1995, **39**, 697–712.
32 D. W. Adrian and A. J. Giacomin, *J. Rheol.*, 1992, **36**, 1227–1243.
33 R. Mas and A. Magnin, *Rheol. Acta*, 1997, **36**, 49–55.
34 V. Hackley and C. Ferraris, *The use of nomenclature in dispersion science and technology*, US Dept. of Commerce, Technology Administration, National Institute of Standards and Technology, 2001.
35 F. Gadala-Maria and A. Acrivos, *J. Rheol.*, 1980, **24**, 799–814.
36 D. Leighton and A. Acrivos, *J. Fluid Mech.*, 1987, **181**, 415–439.
37 D. Merhi, E. Lemaire, G. Bossis and F. Moukalled, *J. Rheol.*, 2005, **49**, 1429–1448.
38 P. R. Nott and J. F. Brady, *J. Fluid Mech.*, 1994, **275**, 157–199.
39 J. M. Bricker and J. E. Butler, *J. Rheol.*, 2006, **50**, 711–728.
40 B. K. Chapman, University of Notre Dame, 1990.
41 A. I. Leonov, *J. Rheol.*, 1990, **34**, 1039.
42 P. Coussot, A. I. Leonov and J. M. Piau, *J. Non-Newtonian Fluid Mech.*, 1993, **46**, 179–217.
43 F. Yziquel, P. J. Carreau, M. Moan and P. A. Tanguy, *J. Non-Newtonian Fluid Mech.*, 1999, **86**, 133–155.
44 J. J. Stickel, R. J. Phillips and R. L. Powell, *J. Rheol.*, 2006, **50**, 379–413.
45 A. I. Isayev and X. Fan, *J. Rheol.*, 1990, **34**, 35–54.
46 B. J. Maranzano and N. J. Wagner, *J. Chem. Phys.*, 2001, **114**, 10514–10527.
47 A. Fall, N. Huang, F. Bertrand, G. Ovarlez and D. Bonn, *Phys. Rev. Lett.*, 2008, **100**, 018301.
48 D. Lootens, H. van Damme, Y. Hémar and P. Hébraud, *Phys. Rev. Lett.*, 2005, **95**, 268302.
49 R. L. Hoffman, *Adv. Colloid Interface Sci.*, 1982, **17**, 161–184.
50 E. Brown, N. A. Forman, C. S. Orellana, H. Zhang, B. W. Maynor, D. E. Betts, J. M. DeSimone and H. M. Jaeger, *Nat Mater*, 2010, **9**, 220–224.
51 H. A. Barnes, *J. Rheol.*, 1989, **33**, 329–366.
52 K. S. Cho, K. Hyun, K. H. Ahn and S. J. Lee, *J. Rheol.*, 2005, **49**, 747–758.
53 R. H. Ewoldt, A. E. Hosoi and G. H. McKinley, *J. Rheol.*, 2008, **52**, 1427–1458.
54 C. O. Klein, H. W. Spiess, A. Calin, C. Balan and M. Wilhelm, *Macromolecules*, 2007, **40**, 4250–4259.
55 R. Ewoldt and G. McKinley, *Rheol. Acta*, 2010, **49**, 213–219.
56 S. Jarny, N. Roussel, S. Rodts, F. Bertrand, R. Le Roy and P. Coussot, *Cem. Concr. Res.*, 2005, **35**, 1873–1881.
57 A. Acrivos, R. Mauri and X. Fan, *Int. J. Multiphase Flow*, 1993, **19**, 797–802.
58 D. Leighton and A. Acrivos, *Chem. Eng. Sci.*, 1986, **41**, 1377–1384.
59 A. Chryss, S. Bhattacharya and L. Pullum, *Rheol. Acta*, 2005, **45**, 124–131.
60 A. S. Yoshimura and R. K. Prud'homme, *J. Rheol.*, 1988, **32**, 575–584.
61 A. E. Kaiser, A. L. Graham and L. A. Mondy, *J. Non-Newtonian Fluid Mech.*, 2004, **116**, 479–488.
62 D. M. Kalyon, *J. Rheol.*, 2005, **49**, 621–640.
63 S. C. Jana, B. Kapoor and A. Acrivos, *J. Rheol.*, 1995, **39**, 1123–1132.
64 A. Yoshimura and R. K. Prud'homme, *J. Rheol.*, 1988, **32**, 53–67.
65 P. E. Boukany and S.-Q. Wang, *Macromolecules*, 2009, **42**, 2222–2228.
66 L. Heymann, S. Peukert and N. Aksel, *J. Rheol.*, 2002, **46**, 93.
67 K. AtalIk and R. Keunings, *J. Non-Newtonian Fluid Mech.*, 2004, **122**, 107–116.